Journal Pre-proof

New triazine bridged triads based on BODIPY-porphyrin systems: extended absorption, efficient energy transfer and upconverted emission

Marcos C. de Souza, Carla I.M. Santos, Inês Mariz, Bruno da S. Marques, Luana A. Machado, Leandro F. Pedrosa, José A.S. Cavaleiro, Maria da Graça P. M. S. Neves, Ricardo F. Mendes, Filipe A.A. Paz, José M.G. Martinho, Ermelinda Maçôas

Please cite this article as: de Souza MC, Santos CIM, Mariz I, da S. Marques B, Machado LA, Pedrosa LF, Cavaleiro JAS, da Graça P. M. S. Neves M, Mendes RF, Paz FAA, Martinho JMG, Maçôas E, New triazine bridged triads based on BODIPY-porphyrin systems: extended absorption, efficient energy transfer and upconverted emission, *Dyes and Pigments*, https://doi.org/10.1016/j.dyepig.2021.109137.

This is a PDF file of an article that has undergone enhancements after acceptance, such as the addition of a cover page and metadata, and formatting for readability, but it is not yet the definitive version of record. This version will undergo additional copyediting, typesetting and review before it is published in its final form, but we are providing this version to give early visibility of the article. Please note that, during the production process, errors may be discovered which could affect the content, and all legal disclaimers that apply to the journal pertain.

Universidade Federal Fluminense
Instituto de Química
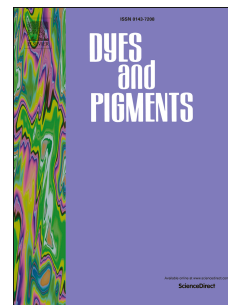
Niterói, October 22th, 2020

To Professor B. Mark Heron and Professor Mark Wainwright,
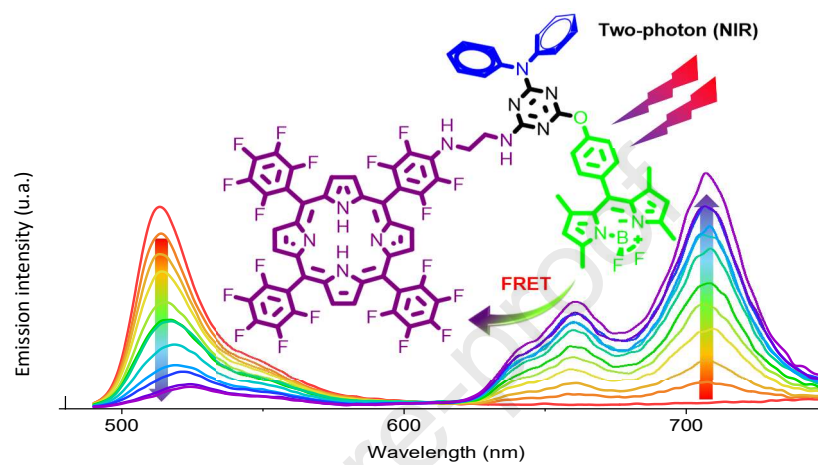Editors-in-Chief of *Dyes and Pigments*

Regarding the manuscript entitled *"*New triazine bridged triads based on BODIPY-porphyrin systems: extended absorption, efficient energy transfer and upconverted emission*"* under submission to *Dyes and Pigments*, follows the authors' statement of contribution:

Corresponding author	Contribution
Marcos C. de Souza	**Project administration, Investigation Writing-review- and editing** Conception, design and analysis
Co-authors	
José A. S. Cavaleiro Maria da Graça P. M. S. Neves	**Supervision, Investigation** Studies and discussion on synthetic pathway to triazine-BODIPY-porphyrin triads 8 and 9.
Carla I. M. Santos Inês Mariz	**Methodology** Synthesis, purification and characterization of porphyrins $TPPF_{20}$, 4 and 5. Experimental photochemical procedures on triazine-BODIPY-porphyrin triads 8 and 9.
Ermelinda Maçôas José M. G. Martinho	**Investigation, Writing-review** Studies and discussion on optical properties of triazine-BODIPY-porphyrin triads 8 and 9.
Filipe A. A. Paz Ricardo F. Mendes	**Methodology, Formal analysis** Recrystallization of compound 7 and resolution of the crystal structure by X-Ray.
Leandro F. Pedrosa Bruno da S. Marques Luana A. Machado	**Investigation, Methodology** Synthesis, purification and characterization of intermediates 6, 7 and triazine-BODIPY-porphyrin triads 8 and 9.

Sincerely,

Marcos Costa de Souza
Doctor in Chemistry, Full professor in Organic Chemistry
Universidade Federal Fluminense – Instituto de Química
marcoscs@id.uff.br

GRAPHICAL ABSTRACT

New triazine bridged triads based on BODIPY-porphyrin systems: extended absorption, efficient energy transfer and upconverted emission

Marcos C. de Souza*[1], Carla I. M. Santos*[2,3], Inês Mariz[2], Bruno da S. Marques[1], Luana A. Machado[1], Leandro F. Pedrosa[1,4], José A. S. Cavaleiro[3], Maria da Graça P. M. S. Neves[3], Ricardo F. Mendes[5], Filipe A. A. Paz[5], José M. G. Martinho[2], Ermelinda Maçôas*[2]

[1] Departamento de Química Orgânica, Instituto de Química. Universidade Federal Fluminense, 24020-141 Niterói, RJ, Brasil.

[2] *CQE, Centro de Química Estrutural*, Instituto Superior Técnico, Av. Rovisco Pais, 1049-001 Lisboa, Portugal.

[3] *LAQV-REQUIMTE, Department of Chemistry,* University of Aveiro, 3810-193 Aveiro, Portugal.

[4] Departamento de Química, Instituto de Ciências Exatas, Universidade Federal Fluminense, 27213-145 Volta Redonda, RJ, Brasil .

[5] *CICECO-Aveiro Institute of Materials,* 3 *Department of Chemistry,* University of Aveiro 3810-193 Aveiro, Portugal.

*Corresponding author: marcoscs@id.uff.br.

Abstract

Two novel triads connecting a BODIPY to ethylenediamine substituted porphyrins via triazine linker have been synthesized and characterized. One of the triads is a linear D-A structure with one BODIPY (D) and one porphyrin (A) bridged by the triazine linker and the other one is a branched A-D_4 structure with the porphyrin core linked to four BODIPY units. The triads show extended absorption in the visible region with contributions from both porphyrin (Soret band centered at 410-430 nm) and BODIPY units (strong absorption at $\approx$ 502 nm) in good agreement with the expected molar ratio. Both triads exhibit linear and nonlinear optical properties featuring an efficient energy transfer from the BODIPY donor to the porphyrin acceptor. The nonlinear upconverted emission properties of the triads were studied by two-photon excitation in the Near-infrared (NIR, 710-930 nm). The maximum two-photon absorption cross-section values for the triads (40-70 GM) are larger than those typically reported in this wavelength range for porphyrins and BODIPY. Both the green emission of BODIPY ($\approx$ 514 nm) and the red emission of porphyrins (650-750 nm) were observed under NIR excitation at 930 nm. The distinct features of triads, namely i) an extended absorption; ii) an efficient energy transfer and iii) the nonlinear upconverted emission featuring a large separation between the excitation and emission wavelengths could be beneficial for application in sensing and imaging procedures.

1. INTRODUCTION

In recent years, a wide range of compounds have been combined to construct multichromophoric and π-conjugated macromolecules with excellent photophysical profiles [1-2]. The presence of conjugated systems improves the efficiency of electron and energy transfer processes [3-4]. Porphyrins, which are tetrapyrrolic ligands with high chemical stability, unique optical properties and strong redox activity are an example of these compounds [5-7]. During the last two decades, such compounds have been extensively studied for use in numerous applications such as solar cells [8-9], chemosensors [10-13], artificial photosynthesis [14], catalysis [15-19], and biomedical applications [20-22]. The absorption spectrum of porphyrins has a typical profile consisting of an intense Soret band at $\lambda = 400–450$ nm followed by a weaker quartet of bands at $\lambda = 550$-650 nm known as the Q bands. The absorption gap between 450-550 nm is a significant limitation for the use of these macrocycles in photocurrent generation phenomena. One of the approaches to expand the absorption profile of porphyrin derivatives is their association to chromophores with strong absorption in the above region. Green chromophores such as 4,4-difluoro-4-bora-3a,4a-diaza-s-indacene, commonly known as BODIPY, with absorption features complementary to porphyrins, are excellent candidates for a synergistic improvement of the intrinsic optical properties of the individual units [4, 23-29]. BODIPY derivatives have been widely used as light harvesting antenna groups due to their excellent photochemical stability, high molar extinction coefficient ($\varepsilon > 6 \times 10^4$ cm^{-1}M^{-1} at the maximum absorption wavelength) and easily tunable optical

and electrochemical properties [30]. However, the light harvesting ability of BODIPY fluorophores is also limited by their typically narrow absorption spectra. Panchromaticity can be achieved by coupling the BODIPY fluorophores with porphyrins. In addition, the preparation of compounds carrying multiple BODIPY units [31-33] can increase the amount of light that is collected by molecular chromophores avoiding undesired effects associated with aggregation in highly concentrated films.

BODIPY fluorophores are also particularly popular in bioimaging and sensing applications due to their near unitary fluorescence quantum yield [34-36]. However, like most organic dyes, their small Stokes shift (10-20 nm) limits the signal-to-noise ratio due to reabsorptions of emitted photons and cross-talk between the excitation source and the fluorescent emission. In this sense, molecules containing both porphyrin and BODIPY units are promising [37-40], and have been the focus of our recent effort to achieve conjugates able to combine the properties of photosensitizers (PS) for photodynamic therapy (PDT) with those of fluorescent markers for biologic studies by exploring efficient intramolecular energy transfer processes and enhanced optoelectronic properties in the blue-green region of the spectrum.

For the construction of the conjugates, we selected 1,3,5-triazine as the linker between the BODIPY and the porphyrin units due to its suitability to join up to three substituents of interest, according to the well-known temperature-dependent stepwise substitutions of the three Cl atoms from the starting cyanuric chloride [41]. In fact, triazine bridged triads having covalently bonded porphyrin and/or BODIPY constituents have been considered in the literature as promising agents in fast

transfer systems [42] and in dye sensitized solar cells (DSSC) [43-45]. In the present study we constructed a fluorescent framework that can accommodate a combination of three different functional groups, where the BODIPY block acts as the fluorophore energy donor (D), the porphyrin core serves as the energy
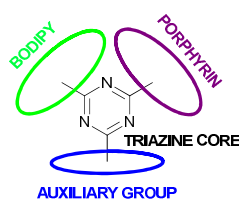
acceptor/photosensitizer (A) and the third substituent functions as an auxiliary group (**Figure 1**).

Figure 1. General framework highlighting triazine bridged triads.

Two triads were synthesized, a linear D-A structure with one BODIPY and one porphyrin unit bridged by the triazine linker and one branched A-D$_4$ structure with the porphyrin core linked to four BODIPY units. The structure and optical properties of the triads were fully characterized. The nonlinear upconverted emission properties of the triads where studied by two-photon excitation in the Near-infrared (NIR, 730-930 nm). NIR excitation is of outmost convenience for the use of fluorophores in high resolution imaging of 3D samples (e.g. *in vitro* imaging of organoids and *in vivo* imaging of small animals) or photosensitizers in scattering media [46-48]. Two-photon induced processes hold also great interest for applications in micromachining and optical power limiting [49]. NIR excitation grants the possibility of penetrating deeper into most materials and thick biological tissue due to reduced absorption and scattering of NIR radiation. The synthesized triads exhibit linear and nonlinear optical properties shaped by the efficient energy transfer from the

BODIPY to the porphyrin. We observed both green and red emission upon excitation at 930 nm featuring a large separation between excitation and emission wavelengths that can be of potential value for sensing and imaging purposes.

2. MATERIAL AND METHODS

2.1. Chemicals

The reagents used for the preparation of porphyrins and BODIPY-Porphyrin conjugates were purchased from Sigma-Aldrich. All solvents were used as received from different commercial sources, with the exception of tetrahydrofuran that was dried using standard procedures.

2.2. Instrumentation

Melting points are uncorrected and were determined on a Büchi B-540 device. The mass spectra were recorded using a ESI-MS MALDI-Micromass Q-TOF2 equipment (potential 40-260 eV). UV–Vis spectra were recorded on a Shimadzu UV-2501PC spectrophotometer. NMR spectra were obtained on a Varian Unity Plus/Bruker Advance DPX spectrometer (300 or 500 MHz): ^{1}H: 300.13 MHz or 500.13 MHz; ^{13}C: 75.47 MHz or 125.76 MHz and ^{19}F: 282.38 MHz or 470.27 MHz. ^{13}C assignments were made based on 2D HSQC and HMBC experiments (delay for long-range J C/H couplings were optimized for 7 Hz). Samples were dissolved in the specified solvent, CDCl$_3$ or DMSO-d$_6$. Chemical shifts were expressed in δ (ppm) for the following references: tetramethylsilane (internal) for ^{1}H and ^{13}C and hexafluorobenzene (external) for ^{19}F. Coupling constants (J) were expressed in Hertz (Hz) and the areas of the signals were obtained by electronic integration. Multiplicity of signals was noted as: s-singlet, d-doublet, t-triplet, q-quartet, quint-quintet, m-multiplet.

2.3. Spectroscopic Measurements

The linear absorption spectra were recorded on a JASCO V-540 spectrophotometer. The fluorescence spectra were recorded using a Horiba Jobin Yvon Fluorlog 3-22 Spectrofluorimeter with a xenon lamp of 450 W. The spectra were recorded in spectroscopic grade dimethylsulfoxide (DMSO) using 5×5 mm quartz cells. The fluorescence quantum yields where determined upon excitation of the Soret band at 422 nm and the BODIPY at 470 nm using 5,10,15,20-tetraphenylporphyrin (TPP) in toluene (Φ = 0.11) and fluorescein at pH 11 as standards (Φ = 0.92) [50].

Two-photon absorption (TPA) spectra were measured in $5-10$ μM DMSO solutions by two-photon fluorescence (TPF) using fluorescein at pH 11 and TPP in CCl_4 as standards, to account for collection efficiency and pulse characteristics [51]. A modified setup that follows closely the one described by Xu and Webb was used to estimate the TPA cross section in the 710–930 nm region. The two-photon emission (TPE) was measured within a narrow wavelength bandwidth selected by the H20Vis Jobin Yvon monochromator placed at the entrance of a PMC-100-4 photomultiplier tube (Becker and Hickl GmbH). The excitation source was a Ti:sapphire laser (Tsunami BB, Spectra-Physics, 710–990 nm, 1.7 W, 100 fs, 82 MHz).

The integrated TPE over the entire emission band was extrapolated using the overall emission spectra measured in the fluorimeter upon excitation at half the two-photon excitation wavelength ($\lambda_{TPA}/2$). The two photon absorption cross section was calculated from the Equation 1:

$$\sigma_2 = (F_2/\Phi Cn)_s \, (\Phi Cn\sigma_2/F_2)_{ref} \qquad (1)$$

8

where F_2 stands for integrated fluorescence intensity, Φ is the fluorescence quantum yield, n refers to the refractive index in solution, C is the concentration, and s and ref are relative to the sample and the TPA reference, respectively. The emission intensity dependence of the excitation power was checked. The relative error of the cross sections values is at most $\pm$ 20%. The fluorescence decays were measured in 5 mm quartz cuvettes by the Single-Photon Timing technique under excitation at 330 nm by collecting the emission at 514 and 700 nm. The excitation source was the 2nd harmonic of a Coherent Radiation Dye laser 700 series (laser dye DCM, 610−680 nm, 130 mW, 5 ps, 4 MHz). The emission was collected at the magic angle by a Jobin Yvon HR320 monochromator (Horiba Jovin Ivon Inc.). The instrument response functions (35–80 ps FWHM) was estimated using a scattering dispersion of colloidal silica in water. Decay curves were stored in 1024 channels with 24.4 to 48.8 ps per channel and an accumulation of 20k counts in the peak channel. The fluorescence decays were analyzed by a nonlinear least-squares reconvolution method using the TRFA DP software by SSTC (Scientific Software Technologies Center, Belarusian State University, Minsk, Belarus).

2.4. Single-crystal X-ray diffraction studies

Single crystals of compound **7** were manually harvested from the crystallization vials and immersed in highly viscous FOMBLIN Y perfluoropolyether vacuum oil (LVAC 140/13, Sigma-Aldrich) to avoid degradation caused by the evaporation of the solvent [52]. Crystals were mounted on either Hampton Research CryoLoops or

MiTeGen MicroLoops, typically with the help of a Stemi 2000 stereomicroscope equipped with Carl Zeiss lenses.

Crystal data were collected at 150(2) K on a Bruker X8 Kappa APEX II CCD area-detector diffractometer (Mo Kα graphite-monochromated radiation, λ = 0.71073 Å) controlled by the APEX3 software package [53] and equipped with an Oxford Cryosystems Series 700 cryostream monitored remotely using the software interface Cryopad [54]. Diffraction images were processed using the software package SAINT+ [55], and data were corrected for absorption by the multiscan semi-empirical method implemented in SADABS 2016/2 [56].

All structures were solved using the algorithm implemented in SHELXT-2014/5 [57], which allowed the immediate location of almost all of the heaviest atoms composing the molecular unit of compound **7**. The remaining missing and misplaced non-hydrogen atoms were located from difference Fourier maps calculated from successive full-matrix least-squares refinement cycles on F^2 using SHELXL from the 2018/3 release [58]. All structural refinements were performed using the graphical interface ShelXle [59].

Hydrogen atoms bound to carbon were placed at their idealized positions using appropriate *HFIX* instructions in SHELXL: *43* (aromatic carbon atoms) and *137* (for the methyl groups). These hydrogen atoms were included in subsequent refinement cycles with isotropic thermal displacements parameters (U_{iso}) fixed at 1.2 (for the former family of hydrogen atoms) or $1.5 \times U_{eq}$ (solely for those associated with the methyl group) of the parent carbon atoms.

The last difference Fourier map synthesis showed for **7**, the highest peak (0.813 eÅ^{-3}) and the deepest hole (-0.392 eÅ^{-3}) located at 1.54 and 0.58 Å from Cl1, respectively. Structural drawings have been created using the software package Crystal Impact Diamond [60].

Crystallographic data (including structure factors) for the crystal structure of **7** has been deposited with the Cambridge Crystallographic Data Centre. Copies of the data can be obtained free of charge on application to CCDC, 12 Union Road, Cambridge CB2 2EZ, U.K. FAX: (+44) 1223 336033. E-mail: deposit@ccdc.cam.ac.uk.

Crystal data for 7: $C_{34}H_{28}BClF_2N_6O$, M = 620.88, monoclinic, space group $P2_1/n$, $Z = 4$, $a = 10.8010(12)$ Å, $b = 18.800(2)$ Å, $c = 15.1359(17)$ Å, $\beta = 105.547(2)$°, $V = 2961.0(6)$ Å^3, μ(Mo-Kα) = 0.182 mm^{-1}, $D_c = 1.393$ g cm^{-3}, red plate with crystal size of 0.19×0.19×0.08 mm^3. Of a total of 43098 reflections collected, 5406 were independent ($R_{int} = 0.0437$). Final $R1 = 0.0600$ [$I > 2\sigma(I)$] and $wR2 = 0.1646$ (all data). Data completeness to theta = 25.24°, 99.7%. CCDC 1951549.

2.5. Synthesis

All reactions sensitive to air or moisture were carried out under N_2. Chemicals of analytical grade were purchased from commercial sources (Sigma-Aldrich or Merck) and were used as received. Solvents were distilled and dried, according to known methodologies. Analytical TLC was carried out on precoated sheets with silica gel (0.2mm thick, Merck), the eluents were prepared volume-by-volume (v/v) and visualization was performed by revelation under ultraviolet radiation (254/366 nm) and/or iodine. Column chromatography was carried out with silica gel 70-230 mesh

11

(Aldrich). 5,10,15,20-tetrakis(pentafluorophenyl)porphyrin (**TPPF$_{20}$**), *tert*-butyl-(2-aminoethyl)carbamate **1**, and 4,4-difluoro-1,3,5,7-tetramethyl-8-(4-hydroxyphenyl)-4-bora-3a,4a-diaza-s-indacene (**BODIPY-OH**) were synthesized as described in the literature [61-63].

Synthesis of TPPF$_{19}$NHCH$_2$CH$_2$NHBoc (2). A 50 mL round-bottom flask containing a magnetic stirring bar was charged with 75 mg of **TPPF$_{20}$** (0.0767 mmol), 12 mg of mono-protected ethylenediamine **1** (0.0767 mmol), 5.5 mg of potassium carbonate (0.0384mmol) and 20 mL of toluene. The mixture was heated at 120 ºC for 24 h under nitrogen atmosphere. The flask was allowed to cool to room temperature and the solvent was removed under reduced pressure. Then, the residue was diluted with chloroform and the organic phase was washed with water (3 x 20 mL). After separation of the organic phase, the solvent was removed under vacuum and the residue was purified by silica gel preparative TLC using chloroform as the eluent. From the first fraction was recovered the starting porphyrin (6%) and compound **2** was obtained from the second fraction in 68% yield, after recrystallization in a mixture of chloroform and methanol. Compound **2** was characterized by ^{1}H and ^{19}F NMR, UV-Vis and MS (Figures S1-S4, Supplementary Information).

Synthesis of TPPF$_{16}$(NHCH$_2$CH$_2$NH-Boc)$_4$ (3). Under inert atmosphere (N$_2$), a round-bottom flask, equipped with a magnetic stirring bar was charged with 75 mg of **TPPF$_{20}$** (0.0767 mmol), 49 mg of *tert*-butyl (2-aminoethyl) carbamate **1** (0.11 mmol), 21 mg of potassium carbonate (0.015 mmol) and 20 mL of toluene. The mixture was refluxed for 72 h until consumption of the starting porphyrin **TPPF$_{20}$**.

After cooling to room temperature, the mixture was diluted with chloroform and washed with water (3 x 20 mL). The organic phase was concentrated under vacuum and the residue was purified by silica gel preparative TLC using as eluent a mixture of chloroform-methanol (9:1) Compound **3** was isolated in 63% and characterized by ^{1}H and ^{19}F NMR and UV-Vis (Figures S5-S8, Supplementary Information).

Synthesis of TPPF$_{19}$NHCH$_2$CH$_2$NH$_2$ (4) and TPPF$_{16}$(NHCH$_2$CH$_2$NH$_2$)$_4$ (5). In a two necked round-bottom flask containing porphyrin **2** or **3** (15 mg) and dichloromethane (1 mL) it was added TFA (1 mL, 1.5 equiv.). The resulting mixture was maintained under stirring for 2 h at room temperature. At this time, TLC showed the complete consumption of the starting material. Then, the reaction was neutralized with an aqueous solution of NaOH 1M until pH to ~12. Finally, the organic product was extracted with chloroform, the organic phase separated, dried over anhydrous Na$_2$SO$_4$ and the solvent removed under reduced pressure. The products (**4** and **5**) were fully characterized by NMR, mass and UV-Vis techniques (Figures S9-S16, Supplementary Information).

Synthesis of 4,6-dichloro-*N,N*-diphenyl-1,3,5-triazin-2-amine (6) [64]**.** Under a nitrogen atmosphere 1.84 g (0.01 mol) of cyanuric chloride and 2.12 g (0.02 mol) of sodium carbonate were dissolved in 20 mL of dry acetone at 0 ºC. To this mixture a solution of 1.42 g (0.0084 mol) of diphenylamine in 10 ml of dry acetone was added dropwise. The reaction was kept at 0 ^{o}C and stirred for about 4 h, monitored by TLC. Upon reaction completion the white precipitate was filtered off and the solvent evaporated under reduced pressure. The remained solid was washed with acetone three times, then purified by column chromatography using CH$_2$Cl$_2$:hexane (2:1) as

the eluent. A pale yellow solid (m.p. 178-179°C) was obtained in 64% yield (see characterization in Figures S17-S18, Supplementary Information).

Synthesis of compound 7. Under nitrogen atmosphere 41.0 mg (0.12 mmol) of **BODIPY-OH** and 38.06 mg (0.12 mmol) of 1,3,5-triazin **6** were dissolved in 9 mL of dry acetone, then 19 mg (0.18 mmol) of sodium carbonate was added. The mixture was stirred at 35 $^{\circ}$C for 27 h, and the evolution of the reaction was monitored by TLC. Upon reaction completion the white precipitate was filtered off and the solvent evaporated under reduced pressure. The crude product was purified by column chromatography using CH_2Cl_2:hexane as the eluent (gradient 2:1 to 4:1). A bright orange-red solid (dec. > 230°C) was obtained in 56% yield and fully characterized by NMR, mass and UV-Vis (see characterization in Figures S19-S25, Supplementary Information).

Synthesis of compound 8. Under nitrogen atmosphere 5.5 mg (0.0054 mmol) of **4** and 3.06 mg (0.0049 mmol) of **7** were dissolved in 7 mL of THF. Two drops of DIPEA were added and the resulting mixture was refluxed for 5 h. Upon reaction completion (monitored by TLC) the white precipitate was filtered off and the solvent was evaporated under reduced pressure. The residue was dissolved in CH_2Cl_2, the organic phase washed twice with water and dried with anhydrous Na_2SO_4 following standard procedures. The crude material was purified by preparative TLC using CH_2Cl_2 as eluent, to give a reddish brown solid in 81% yield from the second upper fraction. The full structural characterization is presented in Figures S26-S31, Supplementary Information.

Synthesis of compound 9. Under nitrogen atmosphere 5.75 mg (0.0051 mmol) of **5** and 11.5 mg (0.0185 mmol) of **7** were dissolved in 6 mL of THF. 20 mg of K_2CO_3 were added and the resulting mixture was refluxed for 28 h. Upon reaction completion (monitored by TLC) the white precipitate was filtered off and the solvent was evaporated under reduced pressure. The residue was dissolved in CH_2Cl_2, the organic phase washed twice with water and dried with anhydrous Na_2SO_4 following standard procedures. The crude material was purified by preparative TLC using THF:hexane (3:2) as the eluent, to give a reddish brown solid in 40% yield. The full structural characterization is presented in Figures S32-S40, Supplementary Information.

3.   RESULTS AND DISCUSSION

8-(4-hydroxyphenyl)-1,3,5,7-tetramethyl BODIPY, herein abbreviated as **BODIPY-OH**, was elected as the fluorophore in our study due to its high fluorescence and appropriate nucleophilicity with respect to cyanuric chloride [32]. **BODIPY-OH** was synthesized in 21% yield by the mechanochemical method described by Laramine et al [65] exploring the green chemistry concept. Diphenylamine was chosen as the auxiliary group, which is expected to modify the chemical and physical properties of the triad with particular emphasis on the solubility. Ultimately two porphyrins derived from the well-studied 5,10,15,20-tetrakis(pentafluorophenyl)porphyrin ($TPPF_{20}$) [61] containing one or four ethylenediamine branches, respectively **4** and **5**, were synthesized (Scheme 1) to complete the triads **8** and **9** presented in Scheme 2. Two-carbon chains separate the porphyrin core from the terminal amino group to minimize the steric interference

towards the nucleophilic substitution reaction over the chlorine atom of the triazine intermediate **7**.

Synthesis of the ethylenediamine substituted fluorophenylporphyrins 4 and 5.

The synthetic access to the amine porphyrins **4** and **5** involved, in both cases, the reaction of 5,10,15,20-tetrakis(pentafluorophenyl)porphyrin (**TPPF$_{20}$**) with the mono-protected Boc-ethylenediamine **1**, prepared according to literature [62], followed by the amine
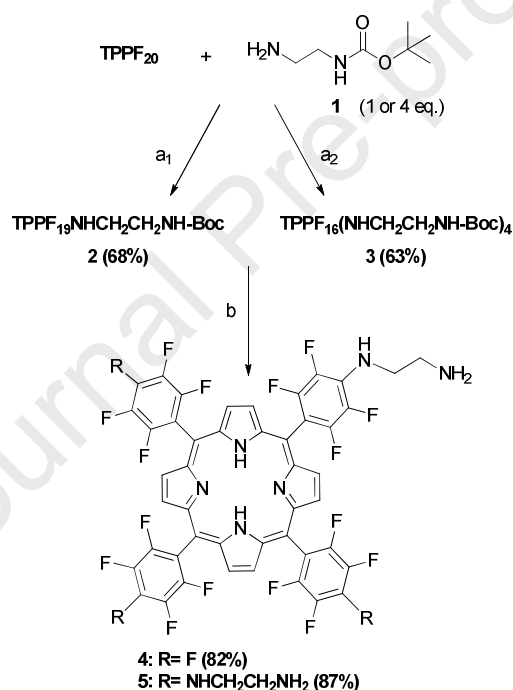
deprotection step (Scheme 1).

Scheme 1. Synthesis of the ethylenediamine substituted fluorophenylporphyrins **4** and **5**. a$_1$) K$_2$CO$_3$, toluene, reflux, 24 h; a$_2$) K$_2$CO$_3$, toluene, reflux, 72 h b) TFA, CH$_2$Cl$_2$, rt, 2 h.

The nucleophilic substitution of one or four *para* fluorine atoms in **TPPF$_{20}$** was controlled by the number of equiv. of the amino derivative **1** and the reactions were performed in

toluene at reflux in the presence of potassium carbonate [62, 66]. The mono-*N*-Boc protected ethylene diamine porphyrin **2** was isolated in 68%, after 24 h of reaction of **TPPF$_{20}$** with 1 equiv. of amine **1**, while the tetra-substituted porphyrin **3** was obtained in 63% after 72 h of reaction using 4 equiv. of the amine. The evolution of both reactions was controlled by TLC and were stopped after verifying the almost consumption of the starting porphyrin accompanied by the formation of the desired main product. The structures of porphyrins **2** and **3** were confirmed by NMR, UV-vis and high-resolution mass spectrometry, see the Supplementary Information, Figures S1-S8. The analysis of ^{1}H NMR spectra (Figures S1 and S5) show in both cases the expected absorption at lower field of the eight *β*-pyrrolic protons of the porphyrin core. In the aliphatic region the resonances of the methylene protons from one alkyl or four alkyl chains appear with the expected pattern - two triplets at δ ~ 3.8 ppm and δ ~ 3.6 ppm. The resonances of the Boc protons appear as a singlet at δ ~ 1.45 ppm and of the two nitrogen internal protons at δ ~ -2.9 ppm as a broad singlet. The analysis of ^{19}F NMR spectra confirms also the expected loss of one *p*-fluorine atom in the case of porphyrin **2** and of four *p*-fluorine atoms in porphyrin **3** (Figures S2 and S6). In the ^{13}C NMR spectra the carbon resonances of the Boc methyl groups are located at δ ~ 29.7 ppm and those due to the remaining methylene carbons are found at δ ~ 47.1 ppm and δ ~ 40.9 ppm. The deprotection of the amino group or groups in porphyrins **2** and **3** in the presence of trifluoroacetic acid (TFA) afforded after the work up the desired porphyrins **4** and **5** in 82 and 87% yields, respectively. The structures of porphyrins **4** and **5** were unambiguously confirmed by 1D, and 2D NMR studies and their molecular formulas by HRMS. In these spectra, the ion peak [M+H]$^+$ at 1015.12537 for **4** and at 1135.31798 for **5**

confirmed the successful cleavage of the *N*-Boc group(s) (Figures S12 and S16). Moreover, in the aliphatic region of their ^{1}H NMR spectra is patent the absence of the signal due to the Boc protons and the presence of two triplets corresponding to the methylene hydrogens at $\delta \sim 3.7$ and 3.1 ppm; a broad singlet due to the resonance of *N*H of the ethylenediamine fragment(s) appear(s) for porphyrin **4** at $\delta \sim 5$ ppm and for porphyrin **5** at $\delta \sim 6.5$ ppm). The resonances of the β-pyrrolic protons as a singlet at δ 9.2 ppm for **5** and as the two doublets at δ 8.9 and 8.8 ppm for porphyrin **4** is on line with the substitution degree (Figures S9 and S13).

Synthesis of triazine-BODIPY-porphyrin triads.

The initial step for the synthesis of the triads **8** and **9** exhibited in Scheme 2 involves the reaction of cyanuric chloride with diphenylamine in the presence of sodium carbonate at 0ºC in dry acetone [64]. Specifically, the choice of this amine as the first group to be connected to the triazine ring is due to its poor nucleophilicity, affording the known intermediate **6** without scrambling with poly-substituted products. Compound **6** was conveniently collected in 64% yield after column chromatography and its mono-substitution pattern confirmed by MS. In the subsequent step, it was performed the replacement of a chlorine atom of **6** using the equivalent amount of **BODIPY-OH** in the presence of sodium carbonate in dry acetone at 35ºC. In the course of the reaction, a new fluorescent orange spot related with the product was observed in the TLC plates (CH$_2$Cl$_2$:hexane 2:1) after 2 hours, along with a considerable amount of **6**. In our case, the consumption of **6** only took place after 27 hours of stirring, and this is significantly longer than the 2 hours

period reported in the literature for similar conditions (see references 31, 32, 64 and 67 as examples). The crude reaction mixture was passed through a chromatography column affording the new compound **7** in 56% yield. In the HRMS-ESI spectrum, the ion peak of **7** [M+H]+ at 621.21247 unequivocally confirms that one BODIPY unity was introduced into compound **6**.

Moreover, the presence of a resonance for two β-pyrrolic protons (δ = 5.98 ppm), two sets of resonances for two methyl groups each (δ = 2.56 ppm and 1.27 ppm) and three sets of resonance for a total of fourteen aryl protons (δ = 7.16-7.39 ppm) in the ^{1}H NMR spectrum, and the characteristic signal at δ = -142.35 in the ^{19}F NMR spectrum corresponding to the BF_2 group, corroborate the expected structure (see the complete NMR assignments in the Supplementary Information).
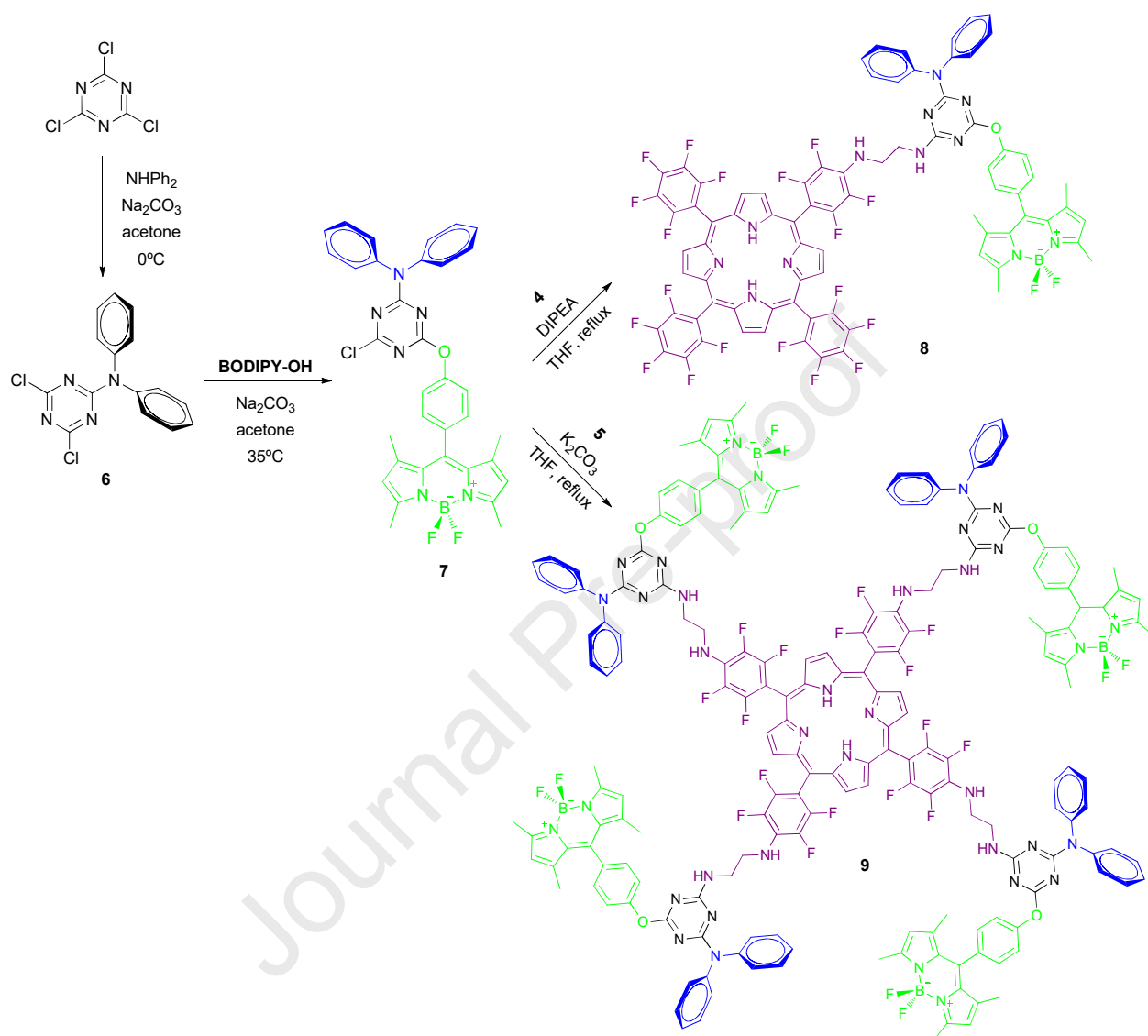
Scheme 2. Synthetic pathway for BODIPY-Porphyrin conjugates **8** and **9**.

Single-crystal X-ray diffraction was also used to fully elucidate the structural features of compound **7** and to unequivocally prove the success of the nucleophilic substitution of **6** with **BODIPY-OH**. Compound **7** crystallizes in the centrosymmetric $P2_1/n$ space group, with the asymmetric unit being composed of a whole molecular unit as depicted in **Figure 2**. The close packing of individual

20

molecular units is mainly driven by the need to effectively fill the available space. A number of weak supramolecular contacts are present within the crystal structure, mainly C–H⋯F hydrogen bonding interactions [between two methyl groups (positions 1 and 7 of the BODIPY system) and F1, and one *o*-phenyl carbon with F2]: $d_{C\cdots F}$ distances found in the 3.187(4)-3.361(4) Å range with the corresponding <(CHF) interaction angles in the range 117-145°. Despite the presence of several
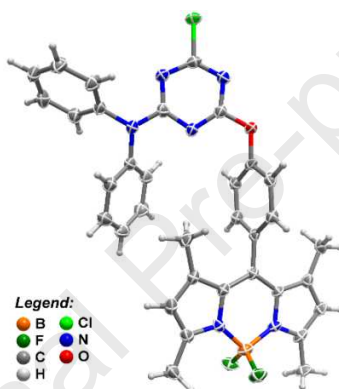
aromatic rings, no structurally-relevant π⋯π contacts were found.

Figure 2. Schematic representation of the molecular unit present in the crystal structure of **7**. Non-hydrogen atoms are represented as thermal ellipsoids drawn at the 50% probability level and hydrogen atoms as small spheres with arbitrary radii.

The last step to achieve triads **8** and **9** consisted in the nucleophilic substitution of the mono- and tetra-amine porphyrins **4** and **5**, respectively, over intermediate **7**. The protocol that has been used by many authors when amino-porphyrins are the nucleophile over cyanuric chloride derivatives makes use of DIPEA as the HCl acceptor [42,43,45,68].

In our experiments, DIPEA reacted as expected in the synthesis of the mono-adduct **8**, but represented a persistent contaminant in the synthesis of the tetra-adduct **9** and so due to that it was replaced by K_2CO_3. In both cases a 10% excess of **4** and **5** was added and the reactions were followed by TLC until the stage when a minimum amount of **BODIPY-OH** was detected. Mono-adduct **8** was isolated in 81% yield by preparative TLC (CH_2Cl_2) after 5 hours in refluxing THF, while completing the total of four substitutions on tetra-adduct **9** required a longer time (28 hours). The latter product was isolated from preparative TLC (THF:hexane 3:2) in 40% yield. In addition to the losses inherent to the TLC purifications of multi substitution reactions, the lower yield of **9** compared to **8** could be attributed to BODIPYs partially substituted porphyrins, whose isolation was not the focus of this work. The structural identities of **8** and **9** were confirmed by ESI- HRMS, ^{1}H, ^{13}C and ^{19}F NMR spectroscopy and the respective spectra are depicted in Supplementary Information (Figures S26-S40). For each compound, the major peak in the ESI-HRMS spectrum appeared as half the calculated molecular weight in agreement with the double-charged $[M+2H]^{2+}$ species.

In the ^{1}H NMR spectrum of **8**, the porphyrin core shows a set of resonances for the eight asymmetric β-pyrrolic protons around δ = 9 ppm and one resonance for two inner NH protons at δ = -2.92 ppm. The resonances due to the ethylenediamine fragment appear as a set of signals between δ = 3.90-3.65 ppm for the four ethylene protons and as two broad peaks for the two NH protons at δ = 5.16 and 4.72 ppm. The BODIPY moiety of **8** showed the same pattern of signals as its precursor **7** and similar chemical shifts. One difference, however, is that the two methyl groups at positions 1 and 7 of the BODIPY system in compound **8** are split into two

resonances at $\delta = 1.25$ and 1.23 ppm, denoting slightly different environments. The tetra-substitution pattern in compound **9** is confirmed, for example, by the 1:4 ratio in the number of inner NH hydrogens of the porphyrin centre (2H, $\delta = -2.89$ ppm) and the peripheral BODIPY β-pyrrolic protons (8H, $= 5.90$ ppm). Highlighted assignments are: a resonance at $\delta = 2.52$ ppm for twenty four methyl protons (positions 3 and 5 of the BODIPY system), two sets of resonance at $\delta = 1.24$ and $\delta = 1.20$ ppm for twelve methyl protons each (positions 1 and 7) and a set of resonance in the range $\delta = 7.09\text{-}7.35$ ppm relative to fifty six aryl protons.

The most distinct feature in the characterization of triads **8** and **9** is observed in the ^{19}F NMR spectra (**Figure 3**). In compound **8** the two fluorine atoms of BF$_2$ give rise to a resonance centred at $\delta = -142.77$ ppm, which is consistent with the integral ratio of the fluoroporphyrin system: six *ortho*-F, six *meta*-F, three *para*-F, two *ortho*'-F and two *meta*'-F. On the other hand, the symmetric compound **9** has a simpler spectrum showing a resonance centred at $\delta = -142.66$ ppm for a total of eight fluorine atoms of four BF$_2$ groups, in agreement with the integral ratio of eight *ortho*-F and eight *meta*-F of the fluoroporphyrin moiety.
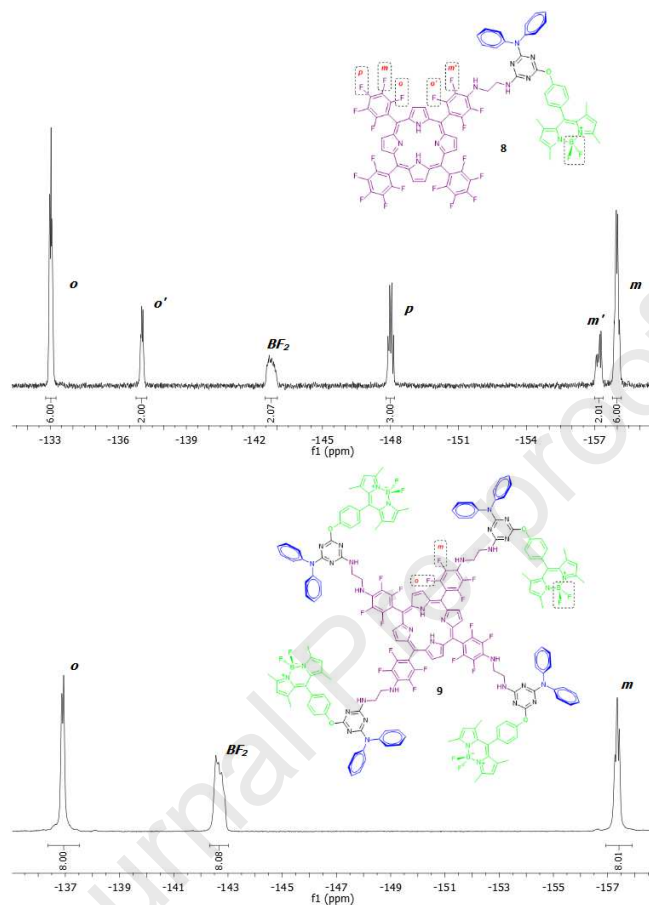
Figure 3. ^{19}F NMR spectra of triads **8** and **9** with integral ratio and fluorine assignment.

Optical properties of BODIPY-porphyrin triads

The UV-Vis absorption and fluorescence emission spectra of the triazine-BODIPY-porphyrin triads are compared with those of the individual units in **Figure 4**. Table 1 presents a summary of the optical properties of compounds **4**, **5**, **7**, **8** and **9**.

Electronic absorption

The ethylenediamine substituted fluorophenylporphyrins **4** and **5** show typical absorption spectra of meso-tetraarylporphyrins with the intense Soret band centred in the 410-430 nm region and being accompanied by less intense Q-bands between 550–650 nm (Figure 4). The maximum molar extinction coefficient of the Soret band is $17.97x10^4$ $M^{-1}cm^{-1}$ for **4** and $12.37x10^4$ $M^{-1}cm^{-1}$ for **5** (Table 1). The BODIPY derivative **7** shows a narrow absorption band centred at 502 nm with molar absorptivity of $7.99x10^4$ $M^{-1}cm^{-1}$ in good agreement with the UV-Vis absorption spectrum of the BODIPY fluorophore.

The absorption spectra of triads **8** and **9** show features of both porphyrin and BODIPY units in good agreement with the expected molar ratio. The molar extinction coefficient of the Soret band in the triads ($15-16x10^4$ $M^{-1}cm^{-1}$) are similar to those of the isolated porphyrins, thus confirming the presence of one porphyrin unit per triad. The molar extinction coefficients of the green absorption of BODIPY in triad **8** (5.9×10^4 $M^{-1}cm^{-1}$) is of the same order of magnitude of derivative **7**, thought it appears to be 30% lower. This band is nearly four times stronger in triad **9** than in triad **8**, thus confirming the tetra-substitution of the porphyrin core in triad **9**.
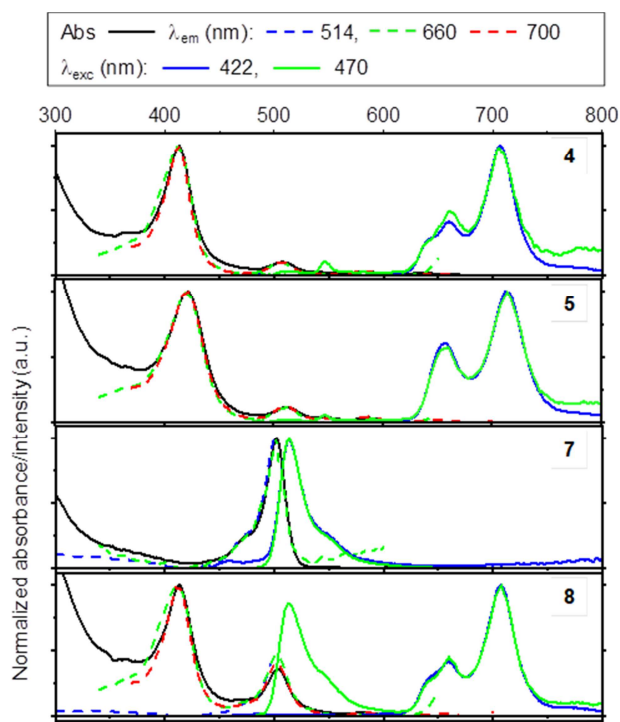

25

Figure 4. Normalized UV-Vis absorption, emission and excitation spectra of compounds **4**, **5**, **7**, **8** and **9** in DMSO. The absorption spectra in straight black trace, the emission spectra upon excitation at 422 nm and 470 nm in straight blue and green traces, respectively, and the excitation spectra recorded upon collection of emission at 514 nm, 660 nm and 700 nm are shown as dashed traces in blue, green and red, respectively.

Steady-state emission

Two emission bands are observed at 660 and 706 nm for compound **4** and 660 and 714 nm for compound **5**. The emission quantum yield Φ of the mono-substituted fluorophenylporphyrin **4** in DMSO (Φ = 3.8%) is slightly lower than that of the tetra-substituted derivative **5** (Φ = 7.4%). The quantum yield of the fluorophenylporphyrin is 2-3 times lower than that of the TPP standard used to estimate the quantum yield. This is a well-known effect of having the hydrogen atoms in the meso-aryl moieties replaced by fluorine, which leads to a larger distortion from planarity. In addition, the halogen atoms promote a spin-orbit coupling that decreases the radiative deactivation pathways while increasing the non-radiative pathways.[69] For compound **7**, the emission of BODIPY is centred at 516 nm with a Stokes shift of only 14 nm and Φ = 65%, considerably higher than that of the porphyrin derivatives.

The photoluminescence spectra of the triads upon excitation at 470 nm feature a narrow band in the green (≈ 515 nm) and a doublet in the red (660/708 nm and 660/718 nm for **8** and **9**) ascribed to the BODIPY and the porphyrin units, respectively. The peak positions of the emission bands in the triads are nearly

coincident with those observed in the isolated components evidencing the lack of conjugation between the porphyrin and the BODIPY units. Emission in the green is exclusively due to direct excitation of the BODIPY. This is supported by the fact that the excitation spectra collected in the green (514 nm) shows only the typical BODIPY absorption band at 502 nm (dashed blue trace in **Figure 4**). On the other hand, emission in the red is observed from either direct excitation of the porphyrin and excitation of the BODIPY followed by an efficient energy transfer from the BODIPY donor (D) to the porphyrin acceptor (A). The energy transfer process is supported by the fact that the excitation spectra of the triads recorded upon collection of the emission in the red (660 or 700 nm) overlaps perfectly with the absorption spectra (dashed green and red lines in **Figure 4**). Furthermore, the good spectra overlap of both emission and excitation spectra of the triads with the spectra of the individual units excludes the formation of emissive charge transfer complexes in both the ground and electronic excited state. This is further supported by the fact that the lifetime of the porphyrin moiety does not changes in the hybrid compared to the free porphyrin, which excludes a charge transfer dynamic quenching. The emission quantum yield of **8** is of the same magnitude order of the quantum yield of porphyrin **4** (Φ = 4.1% and 4.7% upon excitation at 422 and 470 nm, respectively). The emission quantum yield of **9** is about twice higher than that of porphyrin **5** (Φ = 11.3% and 15.9% upon excitation at 422 and 470 nm, respectively). A strong quenching of the BODIPY emission is observed in both triads while the porphyrin

emission efficiency remains similar to that observed in the individual porphyrins **4** and **5**.

Fluorescence Decay Curves

The fluorescence decays were measured in DMSO and fitted with a sum of exponentials after convolution with the experimental response function. The average lifetimes $\bar{\tau} = \frac{\sum a_i \tau_i}{\sum a_i}$ where a_i are the pre-exponential factors and τ_i the lifetimes from the fluorescence decay curves fitting, are collected in Table 1. The average lifetimes are 6.7 and 5.7 ns, respectively for **4** and **5**. The BODIPY derivative **7** has a slightly lower emission lifetime of 4 ns. The energy transfer in the triads results in a faster decay of the green emission of BODIPY (< 1 ns) as compared with emission of derivative **7** (4 ns). As shown in Figure S41 of the Supplementary Information, a very clear fast decay component is observed in the green emission decay of **8** and **9**. The corresponding rise time component in the red emission of the triads is not so evident. Both hybrids show multiexponential red emission decays with average lifetimes in the same range of the individual porphyrins (5-7 ns).

Table 1. Summary of absorption and emission properties of the synthesized compounds: maximum absorption and emission wavelengths (λ_{abs} and $\lambda_{em,}$ nm), photoluminescence emission quantum yields (Φ, %) and average lifetimes ($\bar{\tau}$, ns).

compound	absorption λ_{max}/nm (ε/10^4M^{-1}cm^{-1})	Emission λ_{max}/nm	Φ (%)	$\bar{\tau}$ (ns)
4	413 (17.97), 508 (1.84), 582 (0.60), 632 (0.31)	660, 706	3.8[a]	6.7[c]
5	421 (12.37), 514 (1.67), 547 (0.46), 586 (0.42)	660, 714	7.4[a]	5.7[c]
7	502 (7.99)	516	65.0[b]	4.0[d]
8	413 (16.3), 503 (5.9), 578 (0.48)	514, 660, 708	4.1[a] 4.7[b]	0.3[d] 4.1[c]
9	426 (15.22), 502 (21.20), 548 (0.67), 588 (0.54)	514, 658, 718	11.3[a] 15.9[b]	0.5[d] 7.2[c]

[a] Excitation at 422 nm. [b] Excitation at 470 nm. [c] Emission collected in the red (700 nm). [d] Emission collected in the green (514 nm).

Energy transfer

29

Figure 5 shows that at equimolar concentrations the red emission of the porphyrin upon excitation of the BODIPY unit at 470 nm is significantly stronger in the triads
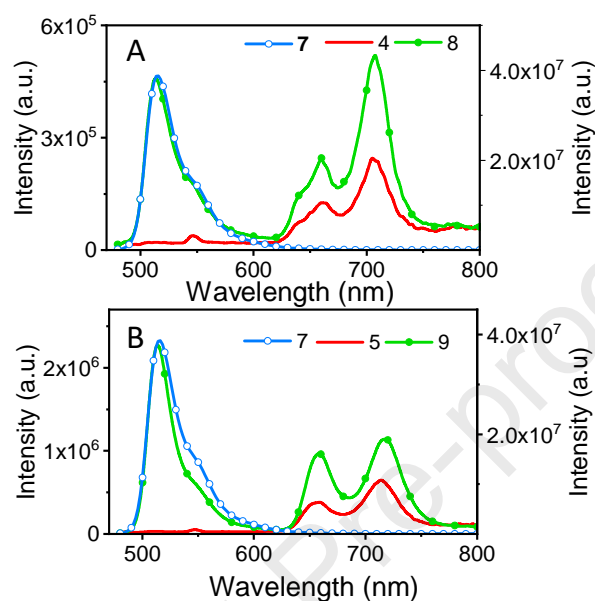
(**8** and **9**) than in the isolated porphyrins (**4** and **5**). This gives a clear evidence of efficient energy transfer from the BODIPY to the porphyrins in the triads. The energy transfer in the triads can be estimated as $E = 1 - \frac{\bar{\tau}_{DA}}{\bar{\tau}_D}$ where $\bar{\tau}_{DA}$ and $\bar{\tau}_D$ refers to the average lifetime of the donor emission measured in the presence (**8** and **9**) and absence (**7**) of the acceptor, respectively. An energy transfer efficiency of nearly 90% is estimated for both triads (92% for **8** and 88% for **9**).

Figure 5. Fluorescence emission of equimolar concentration solutions of the BODIPY (**7**) and porphyrins compared with the corresponding triads in panel A (**4, 7** and **8**) and panel B (**5, 7** and **9**) upon excitation at 470 nm. The intensity of **4, 5, 8** and **9** are read on the left axes while that of derivative **7** is shown on the right axes.

The transfer of excitation energy from an electronic excited molecule (donor) to another (acceptor) is possible if the emission spectrum of the donor partially overlaps with the absorption spectrum of the acceptor. For allowed donor and acceptor transitions, the dipole-dipole term of the expansion of the coulombic interaction is predominant for large donor to acceptor separations. In the limit of very weak coupling, the rate of energy transfer by a dipole-dipole interaction between an energy donor and an acceptor separated by a distance R is given by the Förster Equation 2 [70]:

$$k_{ET} = \frac{1}{\tau_D}\left(\frac{R_0}{R}\right)^6 \qquad (2)$$

where τ_D is the lifetime of the donor in the absence of acceptor and R_0 is the Förster radius at which the rate of energy transfer and decay of the excited donor are equally probable. The Förster radius can be calculated from spectroscopic data of the donor and acceptor molecules, following Equation 3[71]:

$$R_o^6 = 8.79 \times 10^{-5} \left(\frac{\Phi_D \kappa^2}{n^4}\right) \int_0^\infty F_D(\lambda)\varepsilon_A(\lambda)\lambda^4 d\lambda \qquad (3)$$

where Φ_D is the emission quantum yield of the donor, n is the refractive index of the medium, and the integral on the right side of Equation 3 is the overlap integral of the normalized donor emission spectra, $F_D(\lambda)$, with the absorption spectra of the acceptor, $\varepsilon_A(\lambda)$, and κ^2 is an orientation factor between the transition dipole moments of the donor and the acceptor molecules. A $R_0 = 43$ Å is estimated for the BODIPY-Porphyrin donor-acceptor pair in DMSO assuming an orientation factor κ^2

= 2/3 corresponding to freely rotating donor and acceptor dyes. The efficiency of Förster Resonance Energy Transfer (FRET) is given by,

$$E_{FRET} = \frac{k_{ET}}{\frac{1}{\tau_D}+k_{ET}} = \frac{1}{1+\left(\frac{R}{R_0}\right)^6} \qquad (4)$$

which allows the estimation of the average distance between D and A. For an efficiency of 90%, estimated before from the decay times of the donor, a value of R ≈ 30 Å was calculated, which is larger than the distance estimated based on the molecular structure of the conjugates (≈ 20 Å depending on the conformation). The discrepancy in the R values is due to the fact that the donor and acceptor separation is not fixed, but varies with the conformation and Brownian motion of the triads, in which case a distribution of distance has to be considered and the separation R, when evaluated from equation 4, is an apparent separation. Furthermore, the donor and acceptor molecules are not point dipoles and the rotation of the donor and acceptor is not completely free, which introduces uncertainty in the Förster radius, R_0.

Electronic structure calculation of the lowest energy electronic transition of triad **8** and the isodensity surfaces of the frontier molecular orbitals involved (Fig S42) confirm that the mechanism behind the quenching of the emission of BODIPY is a FRET process. The lowest energy transitions involve orbitals localized in the porphyrin fragment (from H or H-1 to L and L+1), orbitals delocalized between this fragment and the triazine bridge (from H-3 to L or L+1), or orbitals localized in the BODIPY fragment (from H-2 to L+2). The lack of orbital overlap between the porphyrin and the BODIPY fragments supports the

assignment of the energy transfer process to a through space dipole – dipole interaction (FRET) rather than through-bond Dexter process.

Nonlinear NIR excitation

The nonlinear emission properties of the triads where studied in the 710-930 nm region. Typical nonlinear two-photon absorption (TPA) cross section of BODIPY and porphyrins in this spectral region have been reported to be below 20 GM [72-74]. The triazine core has also been explored as an electron acceptor unit in the design of small molecules and polymers for upconverted emission based on TPA [75-76]. Triazines have been used in the construction of NIR antenna polymers for two-photon activated volumetric data storage based on energy transfer to photochromic acceptor units [77-78].

The TPA and the upconverted emission spectra of **4**, **7** and **8** are shown in **Figure 6**. The

corresponding results for **5** and **9** are shown in Figure S43 and follow the same trend as for
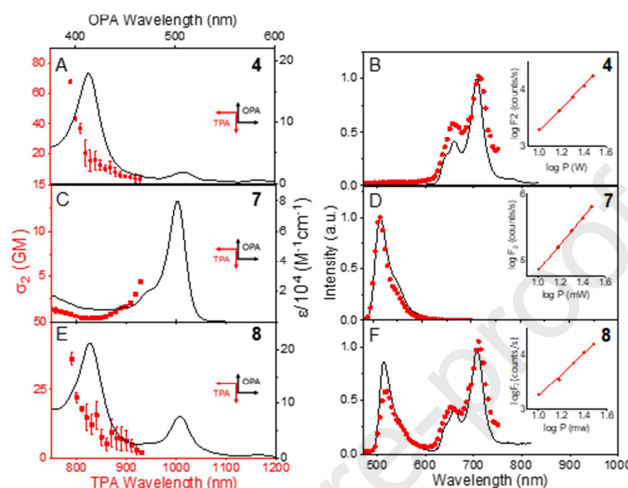
4 and **8**.

Figure 6. Nonlinear two-photon absorption and emission spectra of **4**, **7** and **8**: TPA (red

symbols) and one-photon absorption (OPA, black line) spectra in panels A, C and E on the

left and two-photon emission excited at 930 nm (red symbols) and one-photon emission

excited at 470 nm (black line) in B, D and F on the right. The inserts show the log-log plot

of the NIR excited fluorescence intensity as a function of the excitation power showing a

quadratic dependence (linear fit with a slope of ≈ 2).

The TPA cross-section was determined by two-photon induced fluorescence using well-

known TPA cross-section standards as explained in detail in the experimental section. The

maximum TPA of porphyrin is observed at shorter wavelengths (40-70 GM at 730 nm).

Both **4** and **5** show TPA cross-sections that are at least twice higher than those reported for

the isolated porphyrin units in the 710-930 nm region. In line with earlier reports, the

BODIPY derivative **7** has only a modest TPA cross-section in this wavelength range with the highest value observed at longer wavelengths (5 GM at 930 nm). Noteworthy, the peak of the TPA band of **7** should lay just outside our observation window at 1030 nm (2x516 nm). In the triads the TPA spectra are dominated by the contribution of the porphyrin unit, with maximum TPA cross-sections laying in the same range as those observed for the porphyrins monomer and also peaking at shorter wavelengths. The high TPA cross-sections observed for the triads at 730 nm (36 and 65 GM for triad **8** and **9**, respectively) are in good agreement with the values observed for the porphyrin monomers (40-70 GM). In Figure 4, we showed that the emission spectra upon one-photon excitation depends on the excitation wavelength. The same is true for two-photon induced emission. Nevertheless, the emission should have no memory on the nature of the excitation process, meaning that as long as we introduce the same amount of energy in the system the order of the photon interaction should not affect the nature of final excited state nor its dynamics. Thus, the nonlinear emission spectrum induced at a given excitation wavelength should be equal to the linear emission spectrum at half that wavelength. Indeed, Figure 6(F) shows that the upconverted emission upon two-photon excitation at 930 nm is equal to the down-converted emission spectrum collected upon one-photon excitation at half that wavelength (470 nm). Both the green emission of BODIPY and the red emission of porphyrins are observed under 930 nm excitation. The separation of ≈ 400 nm between NIR excitation and emission in the green can be useful for application in sensing and imaging. On the other hand, excitation in the NIR and emission in the far red might also be of value for applications requiring non-invasive introduction of a certain amounted of energy within scattering media. The inserts in Figure 6 show that for all the compounds the fluorescence emission upon NIR excitation

35

depends quadratically on the excitation power ($\log F_2$ vs log P with a slope of 2), thus confirming that the upconverted emission is due to a two-photon excitation process.

4. CONCLUSION

We synthesized two triads connecting a BODIPY derivative **7** to mono- and tetra-ethylenediamine substituted porphyrins **4** and **5** via a triazine linker. Triad **8** has a linear D-A structure with one BODIPY and one porphyrin unit bridged by the triazine and triad **9** is a branched A-D_4 structure with the porphyrin core linked to four BODIPY units. The structure and optical properties of the triads were evaluated by different techniques namely NMR (^{1}H, ^{19}F, ^{13}C), HRMS, UV-vis and fluorescence. The nonlinear upconverted emission properties of the triads were studied by two-photon excitation in the NIR (710-930 nm). The synthesized triads exhibit linear and nonlinear optical properties shaped by the efficient energy transfer from the BODIPY to the porphyrin. We observed both green and red emission upon excitation in the NIR at 930 nm featuring a large separation between excitation and emission wavelengths that can be of value for application in sensing and imaging.

Supporting information

Additional experimental details, NMR spectra, HPLC-HRMS(ESI-ToF) chromatogram/spectra, absorption and fluorescence spectra, photophysical properties of selected fluorophores, Cartesian coordinates of optimized structures, and Electronic Structure Calculations.

Acknowledgements

References

[1] Xiang N, Huanga X, Fenga X, Liu Y, Zhaoa B, Denga L, Shen P, Fei J, Tan S. The structural modification of thiophene-linked porphyrin sensitizers for dye-sensitized solar

cells. Dyes Pigm.2011; *88*: 75-83.

[2] Ozcemeci I, Gelir A, Gul A. Synthesis and photophysical properties phthalocyanine-pyrene dyads. Dyes Pigm. 2012; *92*: 954-960.

[3] Yan Y, Wu F, Qin J, Xu H, Shi M, Zhou J, Mack J, Fomo G, Nyokong T, Shen Z. Efficient energy transfer in ethynyl bridged corrole–BODIPY dyads. RSC Adv. 2016; 6**:** 72852-72858.

[4] Bucher L, Desbois N, Koukaras EN, Devillers CH, Biswas S, Sharma GD, Gros CP. BODIPY–diketopyrrolopyrrole–porphyrin conjugate small molecules for use in bulk heterojunction solar cells. J. Mater. Chem. A**.** 2018; 6: 8449-8461.

[5] Hiroto S, Miyake Y, Shinokubo H. Synthesis and Functionalization of Porphyrins through Organometallic Methodologies. Chem. Rev. 2017; 117: 2910-3043.

[6] Lu H, Kobayashi N. Optically Active Porphyrin and Phthalocyanine Systems. Chem. Rev. 2016; 116: 6184-6261.

[7] Paolesse R, Nardis S, Monti D, Stefanelli M, Natale C. Porphyrinoids for Chemical Sensor Applications. Chem. Rev. 2017; 117: 2517-2583.

[8] Mendizabal F, Mera Adasme R, Xu WH, Sundholm D. Electronic and optical properties of metalloporphyrins of zinc on TiO_2 cluster in dye-sensitized solar-cells (DSSC). A quantum chemistry study. RSC Adv. 2017; 7: 42677-42684.

[9] Mahmood A, Hu JY, Xiao B, Tang A, Wang X, Zhou E. Recent progress in porphyrin-based materials for organic solar cells. J. Mater. Chem. A**.** 2018; 6:16769-16797.

[10] Gamelas SRD, Gomes ATP, Moura NMM, Faustino MAF, Cavaleiro JAS, Lodeiro C, Veríssimo MIS, Fernandes T, Silva ALD, Gomes MTSR, Neves MGPMS. *N*-Confused

Porphyrin Immobilized on Solid Supports: Synthesis and Metal Ions Sensing Efficacy. Molecules. 2018; 23: 867.

[11] Ding Y, Zhu WH, Xie Y. Development of Ion Chemosensors Based on Porphyrin Analogues. Chem. Rev. 2017; 117: 2203-2256.

[12] Moura NMM, Nunez C, Santos SMM. Faustino MAF, Cavaleiro JAS, Neves MGPMS, Capelo JL, Lodeiro C. Synthesis, Spectroscopy Studies, and Theoretical Calculations of New Fluorescent Probes Based on Pyrazole Containing Porphyrins for Zn(II), Cd(II), and Hg(II) Optical Detection. Inorg. Chem. 2014; 53: 6149-6158.

[13] Santos CIM, Oliveira E, Santos HM, Menezes JCJMDS, Faustino MAF, Cavaleiro JAS, Capelo JL, Neves MGPMS, Lodeiro C. Untangling interactions of a zinc(II) complex containing a coumarin–porphyrin unit with alkaloids in water solutions: a photophysical study. Photochem. Photobiol. Sci. 2015; 14: 757-764.

[14] Nikolaou V, Charisiadis A, Stangel C, Charalambidis G, Coutsolelos AG. Porphyrinoid–Fullerene Hybrids as Candidates in Artificial Photosynthetic Schemes. *C - Journal of Carbon Research*. 2019; 5: 57.

[15] Pereira CF, Simões MMQ, Tomé JPC, Paz FAA. Porphyrin-Based Metal-Organic Frameworks as Heterogeneous Catalysts in Oxidation Reactions. Molecules 2016; 21: 1348.

[16] Castro KADF, Figueira F, Mendes RF, Cavaleiro JAS, Neves MGPMS, Simões MMQ, Paz FAA, Tomé, JPC, Nakagaki S. Copper–Porphyrin–Metal–Organic Frameworks as Oxidative Heterogeneous Catalysts. Chem. Cat. Chem. 2017; 9: 2939-2945.

[17] Neves CMB, Tomé JPC, Hou Z, Dehaen W, Hoogenboom R, Neves MGPMS, Simões MMQ. Oxidation of Monoterpenes Catalysed by a Water-Soluble Mn[III] PEG-Porphyrin in a Biphasic Medium. Chem. Cat. Chem. 2018; 10: 2804-2809.

[18] Silva ES, Moura NMM, Neves MGPMS, Coutinho A, Pietro M, Silva CG, Faria JL. App. Cat. B-Env. 2018; 221: 56-69.

[19] Simões MMQ, Gonzaga DTG, Cardoso MFC, Forezi LSM, Gomes ATPC, Silva FC, Ferreira VF, Neves MGPMS, Cavaleiro JAS. Carbene Transfer Reactions Catalysed by Dyes of the Metalloporphyrin Group. Molecules. 2018: 23(4): 792.

[20] Gomes ATPC, Neves MGPMS, Cavaleiro JAS. Cancer Photodynamic Therapy and Porphyrin-Type Derivatives. An. Acad. Bras. Ciênc. 2018; 90: 993-1026.

[21] Moura NMM, Ramos CIV, Linhares I, Santos SM, Faustino MAF, Almeida A, Cavaleiro JAS, Amado FML, Lodeiro C, Neves MGPMS. Synthesis, characterization and biological evaluation of cationic porphyrin-terpyridine derivatives. RSC Adv.2016; 6: 2046-2069.

[22] Sagrillo FS, Dias C, Gomes ATPC, Faustino MAF, Almeida A, Souza AG, Costa ARP, Boechat FCS, Souza MCBV, Neves MGPMS, Cavaleiro JAS. Synthesis and photodynamic effects of new porphyrin/4-oxoquinoline derivatives in the inactivation of S. aureus. Photochem. Photobiol. Sci. 2019; 18: 1910-1922.

[23] Leonardi MJ, Topka MR, Dinolfo PH. Efficient Förster Resonance Energy Transfer in 1,2,3-Triazole Linked BODIPY-Zn(II) Meso-tetraphenylporphyrin Donor–Acceptor Arrays. Inorg. Chem. 2012; 24: 13114-13122.

[24] Kostereli Z, Ozdemir T, Buyukcakir O, Akkaya EU. Tetrastyryl-BODIPY-Based Dendritic Light Harvester and Estimation of Energy Transfer Efficiency. Org. Lett. 2012; 14: 3636-3639.

[25] Turksoy A, Yildiz D, Akkaya EU. Photosensitization and controlled photosensitization with BODIPY dyes. Coord. Chem. 2019; 379: 47-64.

[26] Kim K, Choi SH, Jeon J, Lee H, Huh JO, Yoo J, Kim JT, Lee C, Lee YS, Churchill DG. Control of On–Off or Off–On Fluorescent and Optical [Cu^{2+}] and [Hg^{2+}] Responses via Formal Me/H Substitution in Fully Characterized Thienyl "Scorpionate"-like BODIPY Systems. Inorg. Chem. 2011; 50: 5351-5360.

[27] Zhang T, Zhu X, Wong WK, Tam HL, Wong WY. Light-Harvesting Ytterbium(III)–Porphyrinate–BODIPY Conjugates: Synthesis, Excitation-Energy Transfer, and Two-Photon-Induced Near-Infrared-Emission Studies. Chem. Eur. J. 2013; 19: 739-748.

[28] Khan TK, Bröring M, Mathur S, Ravikanth M. Coord. *B,B*-Diporphyrinbenzyloxy-BODIPY Dyes: Synthesis and Antenna Effect. Chem. Rev. 2013; 257: 2348-23650.

[29] Khan TK, Ravikanth M. Synthesis and photophysical properties of covalently linked boron dipyrromethene dyads Tetrahedron. 2012; 68: 830-840.

[30] Kursunlu AN. Porphyrin–Bodipy combination: synthesis, characterization and antenna effect. RSC Adv. 2014; 4: 47690-47696.

[31] Qi X, Kim SK, Han SJ, Xu L, Jee AY, Kim HN, Lee C, Kim Y, Lee M, Kim S-J, Yoonynski. A triazine-based BODIPY trimer as a molecular viscometer. J. Supramol. Chem. 2009; 21: 4535-4540.

[32] Zhou W, Guo H, Lin J, Yang J. Multiple BODIPY derivatives with 1,3,5-triazine as core: balance between fluorescence and numbers of BODIPY units. J. Iranian Chem. Soc. 2018;15: 2559-2566.

[33] Yang Z, Kang DH, Lee H, Shin J, Yan W, Rathore B, Kim HR, Kim SJ, Singh H, Liu L, Qu J, Kang C, Kim J S. A Fluorescent Probe for Stimulated Emission Depletion Super-Resolution Imaging of Vicinal-Dithiol-Proteins on Mitochondrial Membrane. Bioconjugate Chem. 2018; 29: 1446-1453.

[34] Machado LA, Souza MC, Silva CM, Yoneda J, Rezende LCD, Emery FS, Simone CA, Júnior ES, Pedrosa LF. On the synthesis, optical and computational studies of novel BODIPY-based phosphoramidate fluorescent dyes J. Fluorine Chem. 2019; 220: 9-15.

[35] Gontijo TB, Freitas RP, Emery FS, Pedrosa LF, JVB Neto, Cavalcanti BC, Pessoa C, King A, Moliner F, Vendrell M, Júnior ENS. On the synthesis of quinone-based BODIPY hybrids: New insights on antitumor activity and mechanism of action in cancer cells. Bioorg. Med. Chem. Lett. 2017; 27: 4446-4456.

[36] Kaur P, Singh K. Recent advances in the application of BODIPY in bioimaging and chemosensing. J. Mat. Chem C. 2019; 37: 11361-11405.

[37] Berksun E, Nar I, Atsay A, Özçeşmeci I, Gelir A, Hamuryudan E. Synthesis and photophysical properties of a porphyrin–BODIPY dyad and a porphyrin–*o*-carborane–BODIPY triad. Inorg. Chem. Front. 2018; 5: 200-207.

[38] Weber MD, Nikolaou V, Wittmann JE, Nikolaou A, Angaridis PA, Charalambidis G, Stangel C, Kahnt A, Coutsolelos AG, Costa RD. Benefits of using BODIPY–porphyrin dyads for developing deep-red lighting sources. Chem. Commun**. 2016; 52: 1602-1605.

[39] Kursunlu AN. Porphyrin–Bodipy combination: synthesis, characterization and antenna effect. RSC Adv. 2014; 4: 47690-47696.

[40] Nikoloudakis E, Karikis K, Han J, Kokotidou C, Charisiadis A, Folias F, Douvas AM, Mitraki A, Charalambidis G, Yan X, Coutsolelos AG. A self-assembly study of PNA–porphyrin and PNA–BODIPY hybrids in mixed solvent systems. Nanoscale. 2019; 11: 3557-3566.

[41] Koc ZE. Complexes of iron(III) and chromium(III) salen and salophen Schiff bases with bridging 1,3,5-triazine derived multidirectional ligands. J. Heterocycl. Chem. 2011; *48*: 769-775.

[42] Lazarides T, Charalambidis G, Vuillamy A, Réglier M, Klontzas E, Froudakis G, Kuhri S, Guldi DM, Coutsolelos AG. Promising Fast Energy Transfer System via an Easy Synthesis: Bodipy–Porphyrin Dyads Connected via a Cyanuric Chloride Bridge, Their Synthesis, and Electrochemical and Photophysical Investigations Inorg. Chem. 2011; *50*: 8926-8936.

[43] Zervaki GE, Agapi N, Vasilis N, Sharma GD, Athanassios CG. "Scorpion"-shaped mono(carboxy)porphyrin-(BODIPY)₂, a novel triazine bridged triad: synthesis, characterization and dye sensitized solar cell (DSSC) applications. J. Mater. Chem. C. 2015; *3*: 5652-3664.

[44] Zhang Q, Sun J, Shang KX, Liu JC, Li RZ, Jin NZ. A dye-sensitized solar cell containing an anchoring porphyrin. J. Coord. Chem. 2017; 70: 780-789.

[45] Sharma GD, Angaridis PA, Pipou S, Zervaki GE, Nikolaou V, Misra R, Coutsolelos AG. Efficient co-sensitization of dye-sensitized solar cells by novel porphyrin/triazine dye and tertiary aryl-amine organic dye. Org. Electron. 2015; 25: 295-307.

[46] Ingaramo M, York AG, Wawrzusin P, Milberg O, Hong A, Weigert R, Patterson GH. Proceedings of the National Academy of Sciences. 2014; 111: 5254-.

[47] Maçôas E, Marcelo G, Pinto S, Caneque T, Cuadro AM, Vaquero JJ, Martinho JMG. A V-shaped cationic dye for nonlinear optical bioimaging. Chem. Commun. 2011; 47: 7374-7376.

[48] Marcelo G, Pinto S, Caneque T, Mariz IFA, Cuadro AM, Vaquero JJ, Martinho J M G, Maçôas EMJ. Nonlinear Emission of Quinolizinium-Based Dyes with Application in Fluorescence Lifetime Imaging. Phys. Chem. A. 2015;119: 2351-2362.

[49] He GS, Tan L-S, Zheng Q, Prasad P N. Multiphoton Absorbing Materials: Molecular Designs, Characterizations, and Applications. Chem. Rev. 2008;108: 1245-1330.

[50] Gradyushko AT, Sevchenko AN, Solovyov KN, Tsvirko MP, Energetics of photophysical processes in chlorophyll-like molecules Photochem. Photobiol. 1970; 11: 387-400.

[51] Makarov NS, Drobizhev M, Rebane A. Two-photon absorption standards in the 550–1600 nm excitation wavelength range. Opt. Express 2008; 16: 4029-4047.

[52] Kottke T, Stalke D. Crystal handling at low temperatures. J. Appl. Crystallogr. 1993, 26, 615-619.

[53] APEX3, Data Collection Software Version 2016.9-0, Bruker AXS, Delft, The Netherlands, 2005-2016.

[54] Cryopad, Remote monitoring and control, Version 1.451, Oxford Cryosystems, Oxford, United Kingdom, 2006.

[55] SAINT+, Data Integration Engine v. 8.37a[©], 1997-2015, Bruker AXS, Madison, Wisconsin, USA.

[56] Krausel L, Herbst-Irmer R, Sheldrick GM, Stalke D. Comparison of silver and molybdenum microfocus X-ray sources for single-crystal structure determination. J. Appl. Crystallogr. 2015; 48: 3-10.

[57] Sheldrick GM. SHELXT - Integrated space-group and crystal-structure determination. Acta Cryst. A. 2015; 71: 3-8.

[58] Sheldrick GM. Crystal structure refinement with SHELXL. Acta Cryst. C. 2015;71:3-8.

[59] Hübschle CB, Sheldrick GM, Dittric B. The synthesis, crystal structure and Hirshfeld analysis of 4-(3,4-dimethylanilino)-*N*-(3,4-dimethylphenyl)quinoline-3-carboxamide. J. Appl. Crystallogr. 2011; 44: 1281-1284.

[60] Brandenburg K. DIAMOND, Version 3.0a, Crystal Impact GbR, 1997-2014.

[61] Costa JIT, Tomé AC, Neves MGPMS, Cavaleiro, JAS. 5,10,15,20-tetrakis(pentafluorophenyl)porphyrin: a versatile platform to novel porphyrinic materials. J. Porphyrins Phthalocyanines. **2011**; 15: 1116-1133.

[62] Zhang LB, Ma Y, Li, D, Li, Li, G, Shi Z, Feng S. A strategy toward constructing a bifunctionalized MOF catalyst: post-synthetic modification of MOFs on organic ligands and coordinatively unsaturated metal sites. Chem. Commun. 2012; 48: 6151-6153.

[63] Tomé JPC, Neves MGPMS, Tomé AC, Cavaleiro JAS, Mendonça AF, Pegado IN, Duarte R, Valdeira ML. Synthesis of glycoporphyrin derivatives and their antiviral activity against herpes simplex virus types 1 and 2. Bioorg. Med. Chem. 2005; 13: 3878-3888.

[64] Su X, Yi Y, Tao J, Qi H, Li D. Synergistic effect between a novel triazine charring agent and ammonium polyphosphate on flame retardancy and thermal behavior of polypropylene Polym. Degrad. Stabil. 2014; 105: 12-20.

[65] Laramie P, Dzyuba JV. Expeditious, mechanochemical synthesis of BODIPY dyes. Beilstein J. Org. Chem. 2013;9: 786-790.

[66] Pedrosa LF, Souza MC, Faustino MAF, Neves MGPMS, Silva AMS, Tomé AC, Ferreira VF, Cavaleiro JAS. Porphyrin–Phosphoramidate Conjugates: Synthesis, Photostability and Singlet Oxygen Generation. Aust. J. Chem. 2011; 6: 939-944.

[67] Xiong Y, Zheng S, Zhu L, Guo H, Yang F. Novel liquid crystals with high fluorescence: Synthesis, mesomorphic and photophysical properties of cholesterol-triazine-BODIPY trimers. J. Mol. Structure 2018; 1164: 311-316.

[68] Zervaki GE, Roy MS, Panda MK, Angaridis PA, Chrissos E, Sharma GD, Coutsolelos AG. Efficient Sensitization of Dye-Sensitized Solar Cells by Novel Triazine-Bridged Porphyrin–Porphyrin Dyads. Inorg. Chem. 2013; 52: 9813-9825.

[69] Azenha EG, Serra AS, Pineiro M, Pereira, MM, Melo JS, Arnaut, LG, Formosinho SJ, Gonsalves AMR. Heavy-atom effects on metalloporfiryns and polyhalogenated porphyrins. Chemical Physics 2002; 280(1-2): 177-190.

[70] Förster, Th. Zwischenmolekulare energiewanderung und fluoreszenz. Ann. Physik 1948; 437(1-2): 55-75.

[71] Lakowicz JR. Principles of Fluorescence Spectroscopy, 3rd edition.

[72] Moura NMM, Mariz IFA, Cavaleiro JAS, Silva AMS, Lodeiro C, Martinho JMG, Macôas EMS, Neves MGPMS. Porphyrin-Oligopyridine Triads: Synthesis and Optical Properties. J. Org. Chem. 2018; 83: 5282-5287.

[73] Makarov NS, Drobizhev M, Rebane V. Two-photon absorption standards in the 550–1600 nm excitation wavelength range. Opt. Express. 2008; 16: 4029-4047.

[74] Zheng Q, Xu G, Prasad PN. Conformationally Restricted Dipyrromethene Boron Difluoride (BODIPY) Dyes: Highly Fluorescent, Multicolored Probes for Cellular Imaging. Chem. Eur. J. 2008; 14: 5812-5819.

[75] Mariz I FA, Maçôas EMS, Martinho JMG, Zou L, Zhou P, Chen X, Qin J. Molecular architecture effects in two-photon absorption: from octupolar molecules to polymers and hybrid polymernanoparticles based on 1,3,5-triazine. J. Mater. Chem. B. 2013; 1: 2169-2177.

[76] Zhang L, Zou L, Xiao J, Zhou P, Zhong C, Chen X, Qin J, Mariz IFA, Maçôas E. Symmetrical and unsymmetrical multibranched D–π–A molecules based on 1,3,5-triazine unit: synthesis and photophysical properties. J. Mater. Chem. 2012; 22: 16781-16790.

[77] Mariz IFA, Siopa F, Rodrigues CAB, Afonso CAM, Chen X, Martinho JMG, Maçôas EMS. A 1,3,5-triazine based polymer as a nonlinear near-infrared antenna for two-photon activated volumetric optical memory devices. J. Mater. Chem. C. 2015; 3: 10775-10782.

[78] Zou L, Liu Y, Ma N, Maçôas E, Martinho, J.M.G, Pettersson, M, Chen X, Qina J. Synthesis and photophysical properties of hyperbranched polyfluorenes containing 2,4,6-tris(thiophen-2-yl)-1.

HIGHLIGHTS

- The new triazine-BODIPY-porphyrin triads show extended absorption in the visible
- **D-A** and **A-D$_4$** triads transfer energy from the BODIPY **D**onor to the porphyrin **A**cceptor
- **D-A** and **A-D$_4$** triads show green and red emission upon excitation in the NIR at 930nm
- Nonlinear upconverted emission can be useful for application in sensing and imaging

Declaration of interests

☒ The authors declare that they have no known competing financial interests or personal relationships that could have appeared to influence the work reported in this paper.

☐The authors declare the following financial interests/personal relationships which may be considered as potential competing interests: